Biosensors and Bioelectronics 155 (2020) 112104

Contents lists available at ScienceDirect

Biosensors and Bioelectronics

journal homepage: http://www.elsevier.com/locate/bios

Switch-conversional ratiometric fluorescence biosensor for miRNA detection

Xian Chen [a,*], Ke Xu [a], Jing Li [a], Ming Yang [a], Xing Li [a], Qin Chen [b], Chunhua Lu [a], Huanghao Yang [a,**]

[a] College of Chemistry, Fuzhou University, Fuzhou, 350116, PR China
[b] Fujian Provincial Cancer Hospital & Fujian Medical University Cancer Hospital, Fuzhou, 350014, PR China

ARTICLE INFO

Keywords:
Switch conversion
Exponential amplification reaction
Ratiometric fluorescence biosensor
Förster resonance energy transfer

ABSTRACT

MicroRNAs play a crucial role in regulating gene expression and cellular function. Reliable detection of miRNA is highly demanded in clinical diagnosis and therapy. Herein, we designed a structure-convertible DNA switch and constructed a novel switch-conversional ratiometric fluorescence biosensor (SCRF biosensor) for highly sensitive miRNA detection by the use of amplicon fragments to convert the structure of the switch. The DNA switch was a sophisticated designed single-strand DNA with a stem-loop structure and modified with two fluorophores (Cy3 and Cy5) and one quencher at specific sites of the switch. Amplicon fragments (c*) were produced by an exponential amplification reaction. When the c* hybridized to the loop of a DNA switch, the structure of the switch would convert, and fluorescence resonance energy transfer occurred between Cy5 and Cy3. Then two fluorescence signals with different trends would be observed. As a result, by the ratio of the two signals, we can quantitatively and quickly detect the target miRNA with the concentration range from 100 fM to 100 nM and the excellent detection limit down to 70.9 fM, providing this new SCRF biosensor broad application prospects.

1. Introduction

MicroRNAs (miRNAs) are endogenous, evolutionarily conserved, non-coding single-stranded RNAs (Eulalio et al., 2008). These miRNAs not only play a key role in regulating transcription, but also serve as essential regulators in a wide range of biological processes, such as cell proliferation, differentiation, apoptosis, and hematopoiesis (Cerny and Quesenberry, 2004; Wang et al., 2010; Georgantas III et al., 2007). The expression of miRNAs may be closely related to many human diseases (Guire et al., 2013; Tricoli and Jacobson, 2007). Therefore, the detection of miRNA is of great significance for the diagnosis of diseases and functional analysis of molecular biology.

Due to their small size, low concentration and high sequence similarity between family members, miRNAs are very challenging to be detected (Causa et al., 2015; Ganguly et al., 2018; Dong et al., 2013; Wu et al., 2018). Many detection methods have been developed for miRNAs, such as northern blotting (Torres et al., 2011; Várallyay et al., 2008), quantitative reverse-transcriptase polymerase chain reaction (qRT-PCR) (Kelnar et al., 2014), surface plasmon resonance imaging (SPRi) (Fang et al., 2006; Wood et al., 2013), nanoparticle-based colorimetric detection (Persano et al., 2016), surface-enhanced Raman scattering (SERS) (Driskell et al., 2008; Sun and Li, 2018), and electrochemical detection (Yang et al., 2009; Labib et al., 2013; Masud et al., 2019). Besides, the fluorescence detection method (Tonelli et al., 2006; Lu et al., 2012) has attracted more and more attention in the field of miRNAs sensing because of its high speed, easy operation, and capacity to high-throughput screening. However, compared with methods such as electrochemical detection and electrochemiluminescence detection (Koo et al., 2016; Li et al., 2017; Azzouzi et al., 2019; Chen et al., 2019), the sensitivity of fluorescence detection is not ideal. Therefore, researchers have developed some techniques for signal amplification to improve the sensitivity of fluorescence sensors, such as exponential amplification reaction (EXPAR) (Van Ness et al., 2003; Jia et al., 2010), rolling circle amplification (RCA) (Harcourt and Kool, 2012; Deng et al., 2014; Tang et al., 2018), catalytic hairpin assembly (CHA) (Yang et al., 2019; Mudiyanselage et al., 2018; Wei et al., 2016), hybridization chain reaction (HCR) (Mansourian et al., 2017), enzymatic amplification (Robertson et al., 2017; Luby and Zheng, 2017), and so on (Li et al.,

* Corresponding author.
** Corresponding author.
E-mail addresses: xchen_fzu@126.com (X. Chen), hhyang@fzu.edu.cn (H. Yang).

https://doi.org/10.1016/j.bios.2020.112104
Received 5 November 2019; Received in revised form 31 January 2020; Accepted 17 February 2020
Available online 17 February 2020

2011; Yin et al., 2012; Degliangeli et al., 2014). These fluorescence-based amplification methods effectively improve detection performance, exhibiting better selectivity and sensitivity.

However, most of these fluorescence biosensors are usually based on a single signal change, prone to false positive or false negative detection results, reducing the reliability of the results. Therefore, the ratiometric fluorescence detection method becomes more attractive (Bigdeli et al., 2019; Yi et al., 2017; Xia et al., 2018; Liu et al., 2017). Förster resonance energy transfer (FRET) can be used as a proficient approach to design a ratiometric fluorescence biosensor. FRET is an energy transfer process between a donor fluorophore and an acceptor chromophore (Lakowicz, 2006). The occurrence of FRET is mainly related to two factors. One is that the emission spectrum of the donor and the absorption spectrum of the acceptor overlap. Another is that the distance between the donor and the acceptor is less than 10 nm (Berney and Danuser, 2003; Clapp et al., 2004; Corry et al., 2005; Sun et al., 2011). For instance, the emission spectrum of the fluorophores Cy3 ranges approximately from 540 nm to 650 nm, while the absorption spectrum of the fluorophores Cy5 ranges around from 550 nm to 660 nm (Malicka et al., 2003). Therefore, FRET occurs when the distance between Cy3 and Cy5 is less than 10 nm. Besides, when the distance between Cy3 and Cy5 changes, the donor and acceptor signals also change correspondingly. The ratiometric fluorescence result comes from the ratio of the receptor signal to the donor signal. Consequently, the detection result comes from the ratio of the two signals, which significantly enhances the reliability, comparing with the effect that comes from only one signal.

Although the ratiometric fluorescence method is more reliable than most of the traditional fluorescence methods, the sensitivity of the ratiometric method is unsatisfactory due to the limited sensitivity of fluorescence detection. Therefore, researchers are committed to developing some FRET-based amplification methods to improve sensitivity (Hwang et al., 2019; Qiu et al., 2018). However, compared with methods such as electrochemical and electrochemiluminescence, there is still potential for improved sensitivity. Consequently, we designed a structure-convertible DNA switch and constructed a novel switch-conversional ratiometric fluorescence biosensor (SCRF biosensor), which can use an amplicon fragment to convert the structure of the DNA switch for highly sensitive ratiometric fluorescence detection.

As shown in Part one of Scheme 1, we intended to produce enough amplicon fragments by EXPAR at first. In the presence of a target, it can hybridize with the 3' terminus of the template and then extend along with it in the presence of Vent (exo$^-$) DNA polymerase and deoxyribonucleotide triphosphates (dNTPs) to form double-stranded DNA (dsDNA). The middle part of the dsDNA contains the recognition site of the nicking enzyme Nt.BstNBI. The nicking enzyme recognizes the site and cleaves the central position of the upper DNA strand (the upper black sequence). The upper cleaved DNA strand will extend along with the lower template again by the polymerase, and the downstream strand c* (the amplicon fragment) will be displaced and released. As a result of continuous nicking, polymerization, and displacement cycles, more and more amplicon fragments c* are produced successfully. In the meantime, every c* can participate in the switch conversion (Part two).

As shown in Part two of Scheme 1, the switch is a sophisticated designed single-strand DNA with a stem-loop structure. Two fluorophores (Cy3 and Cy5) and one quencher are respectively modified at specific sites of the switch. Before c* hybridizes with the switch, only Cy3 emits a fluorescence signal, while Cy5 is quenched by the quencher, at which point the switch is "off". When c* hybridizes to the loop of the switch, the structure of the switch will convert. Cy5 will be away from the quencher and close to Cy3. Then, fluorescence resonance energy transfer occurs between Cy5 and Cy3. As a result, the fluorescence signal of Cy3 decreases, while Cy5 emits a fluorescence signal. At this time, the switch is "on". The fluorescence spectra of Cy3 and Cy5 can be obtained by one measurement. Finally, we achieve the ratiometric fluorescence signal by the fluorescence intensity corresponding to Cy5 and Cy3 in the same curve.

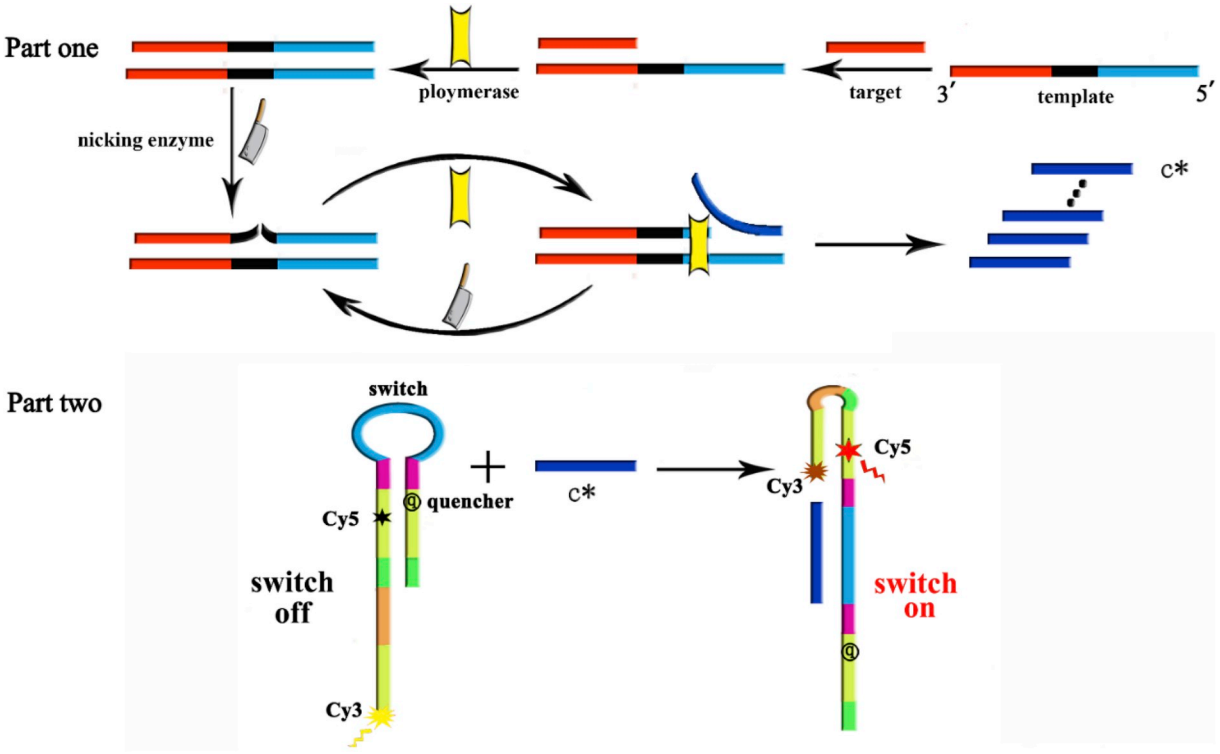

Scheme 1. SCRF Biosensor for let-7a Detection by EXPAR and Switch Conversion.

2. Material and methods

2.1. Reagents and instruments

HPLC-purified oligonucleotides (All the oligonucleotide sequences used in this work are listed in Table S1 of the Supporting Information, SI.), Acryl/Bis 30% Solution, 5 × TBE Buffer (445 mM Tris, 445 mM Boric acid, 10 mM EDTA, pH 8.3), 1 × TBE Buffer (premixed powder, 89 mM Tris-boric, 2 mM EDTA, pH = 8.2–8.4@ 25 °C) and 1 M Tris-HCl Solution, pH 8.0 were obtained from Sangon Biotech Co., Ltd. (Shanghai, China). The pH of all the buffers used in this experiment was adjusted by 0.1 M NaOH and 0.1 M HCl with the pH meter. The pH meter was obtained from Ke Yuan Co., Ltd. (Fujian, China). Vent (exo⁻) DNA polymerase, the nicking endonuclease Nt.BstNBI, 10 × NEBuffer 3.1 (1000 mM NaCl, 500 mM Tris–HCl, 100 mM $MgCl_2$, 1000 μg/mL BSA, pH = 7.9 @25 °C), 10 × ThermoPol buffer (200 mM Tris–HCl, 100 mM KCl, 100 mM $(NH_4)_2SO_4$, 20 mM $MgSO_4$, 1% Triton X-100, pH = 8.8@ 25 °C), RNase inhibitor and dNTPs were purchased from New England Biolabs (Beijing, China). Ammonium persulfate, N, N, N′, N′-Tetramethylethylenediamine, Magnesium Chloride, and Sodium Hydroxide were purchased from Sigma Aldrich Trading Co., Ltd. (Shanghai, China). Hydrochloric acid was purchased by Sinopharm Chemical Reagent Co., Ltd. (Shanghai, China). GelRed was purchased from Life iLab Biotech Co., Ltd. (Shanghai, China). 6 × TriTrack DNA Loading Dye was purchased from Thermo Fisher Scientific Co., Ltd. (Shanghai China). Human real serum samples were obtained from Fujian Provincial Cancer Hospital (Fujian, China). Fluorescence cuvettes were purchased from Yixing Purshee Optical Elements Co., Ltd. (Jiangsu, China). PCR Tubes were purchased from Wuxi NEST Biotechnology Co., Ltd. (Jiangsu, China). The fluorescence intensities were acquired on a Cary Eclipse fluorescence spectrophotometer (Agilent Technologies, Malaysia). Gel images were captured using a ChemiDoc System from Bio-Rad Laboratories (Shanghai, China). The experimental ultrapure water was obtained from the CascadaTM laboratory water treatment system (Jiangsu, China).

2.2. Gel electrophoresis analysis

Gel electrophoresis analysis was performed to characterize the EXPAR process in 1 × TBE buffer at a constant potential of 100 V for 70 min. The gel was visualized by ChemiDocTM Touch Imaging System.

2.3. Multiparametric optimization

Several parameters were investigated to improve the SCRF biosensor performance. In the process of EXPAR, we optimized the concentrations of the amplification template, Vent (exo⁻) DNA polymerase, and Nt.BstNBI, as well as the time of EXPAR. In the switch conversion process, we optimized the concentration of the switch and the hybridization time between amplificons c* and switches.

In the amplification template optimization, the corresponding reaction conditions were switch: 250 nM; Vent (exo⁻) DNA polymerase: 0.05 U/μL; Nt.BstNBI: 0.4 U/μL; the EXPAR temperature: 55 °C; the EXPAR time: 40 min. In Vent (exo⁻) DNA polymerase optimization, the corresponding reaction conditions were the amplification template: 0.1 μM; switch: 250 nM; Nt.BstNBI: 0.4 U/μL; the EXPAR temperature: 55 °C; the EXPAR time: 40 min. The concentrations of the target were 1 nM for all optimization procedures. The conditions in the other optimization process were the same as mentioned above, and only the condition to be optimized was changed.

2.4. Isothermal exponential amplification assay

The reaction mixtures for the EXPAR were prepared on ice separately as solution A and solution B. Solution A consisted of NEBuffer, the amplification template, dNTPs, and the target; solution B consisted of ThermoPol buffer, the nicking endonuclease Nt.BstNBI, Vent (exo⁻) DNA polymerase, and ultrapure water. Firstly, we mixed solution A and solution B to obtain the mixing solution. Then the mixing solution was immediately incubated at 55 °C for 40 min. After that, the mixing solution was incubated at 80 °C for 20 min to inactivate Vent (exo⁻) DNA polymerase and Nt.BstNBI. The EXPAR was performed in a volume of 50 μL containing targets (various concentrations), 0.5 × NEBuffer, 0.1 μM amplification template, 300 μM dNTPs, 1 × ThermoPol buffer, 0.4 U/μL nicking endonuclease Nt.BstNBI, and 0.05 U/μL Vent (exo⁻) DNA polymerase.

2.5. Fluorescence measurement

The mixing solution (25 μL) after EXPAR was mixed with the switch solution (250 nM) in an equal volume and incubated for 60 min before being transferred to a fluorescence cuvette. A Cary Eclipse fluorescence spectrophotometer was used to measure the fluorescence spectra. In real-time measurement, the excitation wavelength of Cy3 was 512 nm, and the emission wavelength reached a maximum at 560 nm. The absorption wavelength range of Cy5 was between 532 and 750 nm, and its maximum emission wavelength measured in real-time was 662 nm. The emission spectrum of Cy3 overlapped with the absorption spectrum of Cy5. The slit width of excitation was kept at 5.0 nm, and the slit width of emission was kept at 10.0 nm.

2.6. Real samples analysis

The serum sample without detectable let-7a was RNase inhibitor-treated. Then the obtained sample solution was diluted 100 times with ultrapure water for the recovery experiments. The detection method was the same as described above, and all experiments were performed under optimal conditions. Recovery experiments for three different target concentrations (100 fM, 1 pM, and 10 pM) were conducted with a standard addition method. RSD (relative standard deviation) was calculated by three independent experiments.

3. Results and discussion

3.1. Gel electrophoresis assay

Gel electrophoresis analysis was conducted to demonstrate and

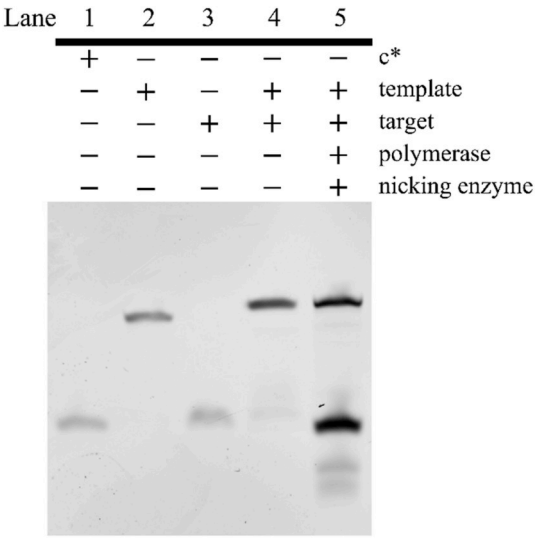

Fig. 1. Gel analysis image of the EXPAR process. Lane 1: c* (0.5 μM) only; Lane 2: template (0.5 μM) only; Lane 3: target (0.5 μM) only; Lane 4: target (0.5 μM) + template (0.5 μM); Lane 5: target (0.5 μM) + template (0.5 μM) + polymerase (0.05 U/μL) + nicking enzyme (0.4 U/μL).

testify the EXPAR process (Fig. 1). The band in lane 1 represented the amplification product c*. The bands in lanes 2 and 3 represented the template and the target, respectively. Compared with bands in lane 2 and 3, the upper band in lane 4 indicated that most of the templates and targets had hybridized together, while the lower indistinct band in lane 4 suggested that only a tiny number of targets had not hybridized to the templates. After the addition of the nicking enzyme and the polymerase to lane 5, a broad and superbright band could be seen in lane 5 under constant sample concentration of target and template, indicating that a large number of c* were amplified successfully. Besides, during the amplification process, the polymerase moved along the template and replicated the template to generate a recognition site for the nicking enzyme. Then the nicking enzyme may cleave the fragment at the recognition site before the polymerase completely replicated the template. Therefore, these fragments cleaved earlier can be observed in lane 5 and shown as the vague bands below the amplicon band.

3.2. Optimizing reaction conditions in the assay

In the EXPAR process, the concentrations of the amplification template, polymerase, and nicking enzyme were optimized to reach the best performance of this assay. As shown in Fig. 2A, the fluorescence ratio rapidly increased with the increasing of the concentration of the template until the concentration reached 0.1 μM. When the concentration of template increased from 0.1 μM to 0.2 μM, the fluorescence ratio increased indistinctively, since almost all the switches had completed structural conversion. Thus, 0.1 μM was selected as the optimal concentration of the template. In Fig. 2B, when the concentration of Vent (exo⁻) DNA polymerase was increased to 0.05 U/μL, the highest fluorescence ratio was obtained. Then the fluorescence ratio decreased as the concentration rising after that. In Fig. 2C, when the concentration of Nt.BstNBI nicking enzyme was increased to 0.4 U/μL, the highest fluorescence ratio was obtained, and then a decreasing fluorescence ratio was observed. Therefore, 0.05 U/μL and 0.4 U/μL were selected separately as the optimal concentration of Vent (exo⁻) DNA polymerase and Nt.BstNBI nicking enzyme.

The reaction time of EXPAR was optimized as well. As shown in Fig. S1A, the fluorescence ratio increased rapidly within 40 min, and the fluorescence ratio no longer changed significantly when the amplification time was extended to 60 min, indicating that the EXPAR process was saturated. Therefore, we chose 40 min as the optimal reaction time for amplification.

Then, considering the range of the fluorescence spectrophotometer, the concentration of the switch was optimized to reach the best fluorescence intensity before switch conversion. As shown in Fig. 3, when the switch concentration was 250 nM, the fluorescence intensity maximum of Cy3 can be measured within the effective range of the fluorescence spectrophotometer (0–1000 a.u). Therefore, we choose

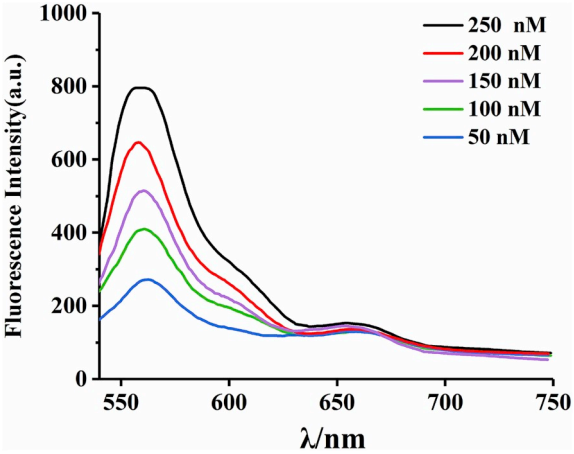

Fig. 3. Changes of the fluorescence signal with different concentrations of the DNA switch. The excitation wavelength and the emission wavelength of Cy3 were 532 and 560 nm, respectively.

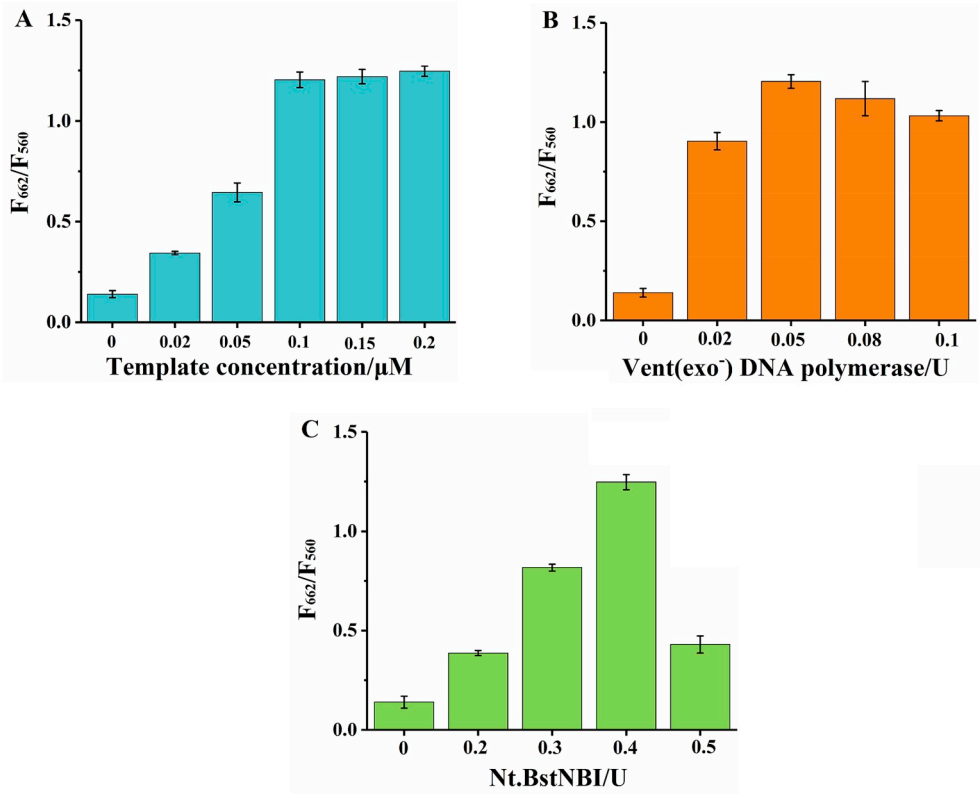

Fig. 2. Optimizing reaction conditions in EXPAR. (A) Changes of fluorescence ratio signal with different concentrations of the template. The corresponding reaction conditions were let-7a: 1 nM; switch: 250 nM; Vent (exo⁻) DNA polymerase: 0.05 U/μL; Nt.BstNBI: 0.4 U/μL; the EXPAR temperature: 55 °C; the EXPAR time: 40 min. (B) Changes of fluorescence ratio signal with different concentrations of the polymerase. The corresponding reaction conditions were let-7a: 1 nM; switch: 250 nM; the amplification template: 0.1 μM; Nt.BstNBI: 0.4 U/μL; the EXPAR temperature: 55 °C; the EXPAR time: 40 min. (C) Changes of fluorescence ratio signal with different concentrations of nicking enzyme. The corresponding reaction conditions were let-7a: 1 nM; switch: 250 nM; the amplification template: 0.1 μM; Vent (exo⁻) DNA polymerase: 0.05 U/μL; the EXPAR temperature: 55 °C; the EXPAR time: 40 min. The excitation wavelength and the emission wavelength were 560 and 662 nm, respectively. Error bars represent the standard deviation from three independent experiments.

250 nM to get the optimal reaction condition.

The effect of reaction time on the DNA switch conversion was studied too. As shown in Fig. S1B, the fluorescence ratio increased rapidly within 60 min, and no longer changed significantly when the conversion time was extended to 90 min. This result indicated that under optimized experimental conditions, approximately 60 min was sufficient to complete the conversion of all DNA switches. Thus, we chose 60 min as the optimal reaction time for the switch conversion.

3.3. Analytical Performance of the SCRF biosensor

Under the optimized conditions, we further investigated the performance of fluorescence ratio response upon different concentrations of the target let-7a. As illustrated in Fig. 4A, as increasing the concentration of target miRNA from 10 fM to 500 nM, the fluorescence intensity of Cy5 increased gradually, and the fluorescence intensity of Cy3 decreased correspondingly. As shown in Fig. 4B, the fluorescence intensity ratio gradually increased with the elevated concentration of target miRNA. Among them, a high linear correlation was obtained between the fluorescence intensity ratio and the logarithm of let-7a concentration from 100 fM to 100 nM. The correlation equation is $F_{662}/F_{560} = 0.2439\ \lg C + 0.4778$ with a correlation coefficient $R^2 = 0.9905$. F_{662}/F_{560} is the ratio of 662 nM–560 nM fluorescence signal, and C is the concentration of let-7a (pM). The detection limit is calculated to be 70.9 fM (see Supporting Information). This SCRF biosensor has an excellent detection limit compared to most reported fluorescence biosensors (Table S3 in Supporting Information).

3.4. Selectivity assay

In order to evaluate the selectivity of the SCRF biosensor, experiments were conducted by different miRNAs, which included miR-21 (100 nM), miR-141 (100 nM), let-7a (1 nM), let-7b (1 nM), and let-7c (1 nM). Among them, let-7b, let-7c, and let-7a belong to the let-7 family (the sequences of let-7b and let-7c have 2-nt and 1-nt variants, respectively, compared to that of let-7a), while miR-21 and miR-141 belong to other different families. As displayed in Fig. 5, in the presence of miR-21 and miR-141, the fluorescence intensity ratio was close to that of the blank sample. In other words, in the absence of the target, even if a high concentration of interference was detected, the signal was close to the background, indicating that the SCRF sensor can be used to distinguish miRNAs from different families. Compared to detecting let-7a of the same concentration (1 nM), the signal of let-7b or let-7c was close to the blank signal. What's more, compared to detecting let-7a only, the negligible change was observed when detecting the mixture 1 (1 nM let-7b and 1 nM let-7a) and mixture 2 (1 nM let-7c and 1 nM let-7a). In the presence of the target, even if mixing the homologous interference of the equal concentration with the target, there was no significant effect on the detection of the target, which demonstrated that the SCRF sensor showed good selectivity among the same families (let-7a, 7b, and 7c). These results indicate that this SCRF biosensor has excellent selectivity for distinguishing let-7a from unrelated miRNAs and other interference sequences belonging to the same family.

3.5. Real-sample assay

In order to study the applicability of the proposed SCRF biosensor in complex biological samples, we carried out recovery experiments using healthy human serum samples to determine the reliability of the SCRF biosensor for let-7a detection. Various concentration of let-7a was added into human serum samples. According to the experimental results, the recoveries were from 99.1% to 102.3%, with a relative standard deviation (RSD, calculated by three independent experiments) of 2.4–4.1% (Table S2 in Supporting Information). These results are satisfactory, demonstrating that the SCRF biosensor has excellent potential for miRNA let-7a detection in real samples.

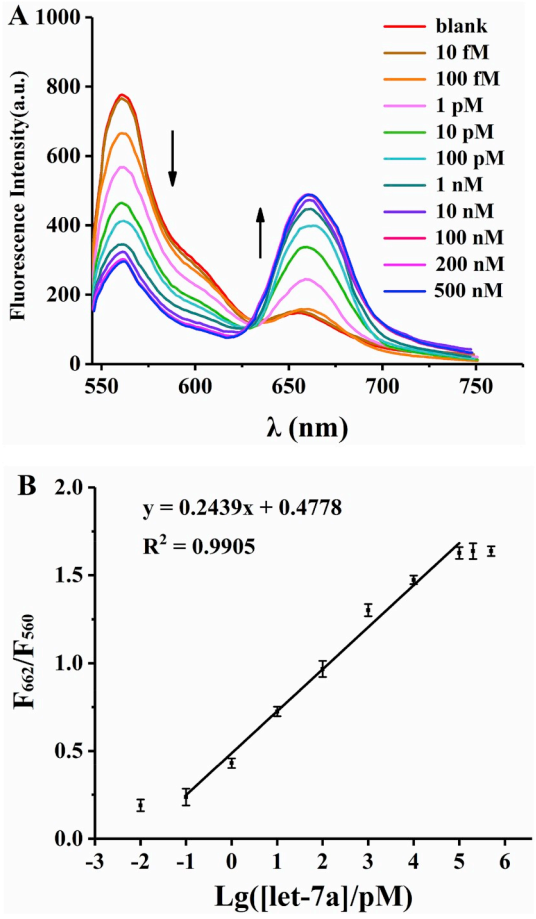

Fig. 4. Analytical Performance of the SCRF biosensor. (A) Fluorescence emission spectra in the presence of let-7a with different concentrations under optimal conditions. (B) The linear correlation between the fluorescence intensity ratio and the logarithm of let-7a concentration from 100 fM to 100 nM. All experiments were performed under optimal conditions. Error bars represent the standard deviation from three independent experiments.

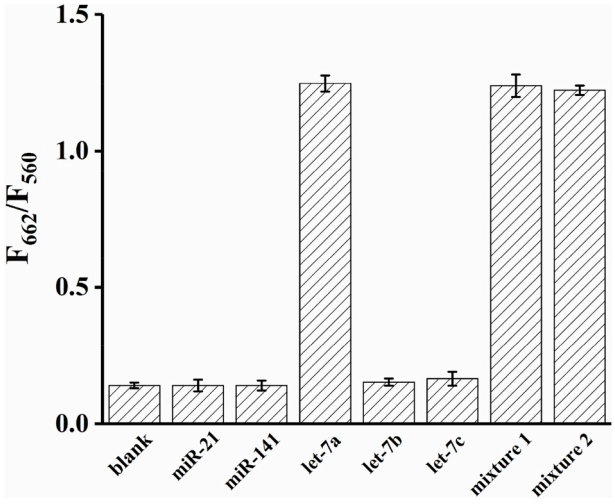

Fig. 5. The selectivity of the SCRF biosensor. The concentrations of miRNAs in let-7 family (let-7a, let-7b, let-7c) were 1 nM. The concentrations of other irrelevant miRNAs (miR-21, miR-141) were 100 nM. All experiments were performed under optimal conditions. Error bars represent the standard deviation from three independent experiments.

4. Conclusions

In summary, we have constructed a novel switch-conversional ratiometric fluorescence biosensor. This sensor is based on an elaborately-designed structure-convertible switch probe, which combines an exponential amplification reaction with fluorescence energy resonance transfer to achieve ratiometric fluorescence detection of the target. A large number of amplicon fragments are harvested using the amplification strategy, thus significantly increasing the sensitivity of the assay with an excellent detection limit of 70.9 fM. Ratiometric fluorescence measurement can offset environmental fluctuations by calculating the emission intensity ratio at two different wavelengths, which further improves the reliability of the assay. What's more, this SCRF biosensor can realize the signal change and detection by the structural conversion of the switch quickly. Besides, the sensor is simple to operate, and the selectivity is satisfactory. Given these advantages, this new SCRF biosensor will have broad application prospects.

Author contributions

The manuscript was written through the contributions of all authors. All authors have approved the final version of the manuscript.

Notes

The authors declare no competing financial interest.

Declaration of competing interest

The authors declare that they have no known competing financial interests or personal relationships that could have appeared to influence the work reported in this paper.

CRediT authorship contribution statement

Xian Chen: Conceptualization, Methodology, Writing - review & editing. **Ke Xu:** Methodology, Investigation, Writing - original draft. **Jing Li:** Investigation. **Ming Yang:** Investigation. **Xing Li:** Investigation. **Qin Chen:** Investigation. **Chunhua Lu:** Writing - review & editing. **Huanghao Yang:** Supervision.

Acknowledgment

This work was financially supported by Department of Education, Fujian Province, China (grant No. JK2017006), and National Natural Science Foundation of China, China (grant No. 21775025, U1705281).

Appendix A. Supplementary data

Supplementary data to this article can be found online at https://doi.org/10.1016/j.bios.2020.112104.

References

Azzouzi, S., Fredj, Z., Turner, A.P.F., Ali, M.B., Mak, W.C., 2019. ACS Sens. 4, 326–334.
Berney, C., Danuser, G., 2003. Biophys. J. 84, 3992–4010.
Bigdeli, A., Ghasemi, F., Abbasi-Moayed, S., Shahrajabian, M., Fahimi-Kashani, N., Jafarinejad, S., Nejad, M.A.F., Hormozi-Nezhad, M.R., 2019. Anal. Chim. Acta 1079, 30–58.
Causa, F., Aliberti, A., Cusano, A.M., Battista, E., Netti, P.A., 2015. J. Am. Chem. Soc. 137, 1758–1761.
Cerny, J., Quesenberry, P.J., 2004. J. Cell. Physiol. 201, 1–16.
Chen, X., Yao, L., Wang, Y.C., Chen, Q., Deng, H., Lin, Z.Y., Yang, H.H., 2019. Biosens. Bioelectron. 131, 274–279.
Clapp, A.R., Medintz, I.L., Mauro, J.M., Fisher, B.R., Bawendi, M.G., Mattoussi, H., 2004. J. Am. Chem. Soc. 126, 301–310.
Corry, B., Jayatilaka, D., Rigby, P., 2005. Biophys. J. 89, 3822–3836.
Degliangeli, F., Kshirsagar, P., Brunetti, V., Pompa, P.P., Fiammengo, R., 2014. J. Am. Chem. Soc. 136, 2264–2267.
Deng, R.J., Tang, L.H., Tian, Q.Q., Wang, Y., Lin, L., Li, J.H., 2014. Angew. Chem. Int. Ed. 53, 2389–2393.
Dong, H.F., Lei, J.P., Ding, L., Wen, Y.Q., Ju, H.X., Zhang, X.J., 2013. Chem. Rev. 113, 6207–6233.
Driskell, J.D., Seto, A.G., Jones, L.P., Jokela, S., Dluhy, R.A., Zhao, Y.P., Tripp, R.A., 2008. Biosens. Bioelectron. 24, 917–922.
Eulalio, A., Huntzinger, E., Izaurralde, E., 2008. Cell 132, 9–14.
Fang, S., Lee, H.J., Wark, A.W., Corn, R.M., 2006. J. Am. Chem. Soc. 128, 14044–14046.
Ganguly, A., Benson, J., Papakonstantinou, P., 2018. ACS Appl. Bio Mater. 1, 1184–1194.
Georgantas III, R.W., Hildreth, R., Morisot, S., Alder, J., Liu, C.G., Heimfeld, S., Calin, G. A., Croce, C.M., Civin, C.I., 2007. Proc. Natl. Acad. Sci. U.S.A. 104, 2750–2755.
Guire, V.D., Robitaille, R., Tétreault, N., Guérin, R., Ménard, C., Bambace, N., Sapieha, P., 2013. Clin. Biochem. 46, 846–860.
Harcourt, E.M., Kool, E.T., 2012. Nucleic Acids Res. 40, e65.
Hwang, K., Mou, Q., Lake, R.J., Xiong, M., Holland, B., Lu, Y., 2019. Inorg. Chem. 58, 13696–13708.
Jia, H.X., Li, Z.P., Liu, C.H., Cheng, Y.Q., 2010. Angew. Chem. Int. Ed. 49, 5498–5501.
Kelnar, K., Peltier, H.J., Leatherbury, N., Stoudemire, J., Bader, A.G., 2014. Anal. Chem. 86, 1534–1542.
Koo, K.M., Carrascosa, L.G., Shiddiky, M.J.A., Trau, M., 2016. Anal. Chem. 88, 2000–2005.
Labib, M., Khan, N., Ghobadloo, S.M., Cheng, J., Pezacki, J.P., Berezovski, M.V., 2013. J. Am. Chem. Soc. 135, 3027–3038.
Lakowicz, J.R., 2006. Principles of Fluorescence Spectroscopy, third ed. Springer, New York.
Li, C.P., Li, Z.P., Jia, H.X., Yan, J.L., 2011. Chem. Commun. 47, 2595–2597.
Li, Z.Y., Lin, Z.F., Wu, X.Y., Chen, H.T., Chai, Y.Q., Yuan, R., 2017. Anal. Chem. 89, 6029–6035.
Liu, Y., Shen, T., Li, J., Gong, H., Chen, C.Y., Chen, X.M., Cai, C.Q., 2017. ACS Sens. 2, 1430–1434.
Lu, Z., Zhang, L., Deng, Y., Li, S., He, N., 2012. Nanoscale 4, 5840–5842.
Luby, B.M., Zheng, G., 2017. Angew. Chem. Int. Ed. 56, 13704–13708.
Malicka, J., Gryczynski, I., Kusba, J., Lakowicz, J.R., 2003. Biopolymers 70, 595–603.
Mansourian, N., Rahaie, M., Hosseini, M., 2017. J. Fluoresc. 27, 1679–1685.
Masud, M.K., Umer, M., Hossain, M.S.A., Yamauchi, Y., Nguyen, N.T., Shiddiky, M.J.A., 2019. Trends Biochem. Sci. 44, 433–452.
Mudiyanselage, A.P.K.K.K., Yu, Q., Leon-Duque, M.A., Zhao, B., Wu, R., You, M., 2018. J. Am. Chem. Soc. 140, 8739–8745.
Persano, S., Guevara, M.L., Wolfram, J., Blanco, E., Shen, H., Ferrari, M., Pompa, P.P., 2016. ACS Omega 1, 448–455.
Qiu, X., Xu, J., Guo, J., Yahia-Ammar, A., Kapetanakis, N.I., Duroux-Richard, I., Unterluggauer, J.J., Golob-Schwarzl, N., Regeard, C., Uzan, C., Gouy, S., DuBow, M., Haybaeck, J., Apparailly, F., Busson, P., Hildebrandt, N., 2018. Chem. Sci. 9, 8046–8055.
Robertson, N.M., Toscano, A.E., LaMantia, V.E., Hizir, M.S., Rana, M., Balcioglu, M., Sheng, J., Yigit, M.V., 2017. Biosens. Bioelectron. 89, 551–557.
Sun, Y., Wallrabe, H., Seo, S.A., Periasamy, A., 2011. ChemPhysChem 12, 462–474.
Sun, Y.D., Li, T., 2018. Anal. Chem. 90, 11614–11621.
Tang, X., Deng, R.J., Sun, Y.P., Ren, X.J., Zhou, M.X., Li, J.H., 2018. Anal. Chem. 90, 10001–10008.
Tonelli, D.D.P., Calegari, F., Fei, J.F., Nomura, T., Osumi, N., Heisenberg, C.P., Huttner, W.B., 2006. Biotechniques 41, 727–732.
Torres, A.G., Fabani, M.M., Vigorito, E., Gait, M.J., 2011. RNA 17, 933–943.
Tricoli, J.V., Jacobson, J.W., 2007. Canc. Res. 67, 4553–4555.
Van Ness, J., Van Ness, L.K., Galas, D.J., 2003. Proc. Natl. Acad. Sci. U.S.A. 100, 4504–4509.
Várallyay, É., Burgyán, J., Havelda, Z., 2008. Nat. Protoc. 3, 190–196.
Wang, X., Zhou, S., Ding, X., Zhu, G., Guo, J., 2010. J. Environ. Sci. Health B. 45, 648–657.
Wei, Y.L., Zhou, W.J., Li, X., Chai, Y.Q., Yuan, R., Xiang, Y., 2016. Biosens. Bioelectron. 77, 416–420.
Wood, J.B., Szyndler, M.W., Halpern, A.R., Cho, K., Corn, R.M., 2013. Langmuir 29, 10868–10873.
Wu, T.T., Yang, Y.M., Cao, Y., Song, Y.C., Xu, L.P., Zhang, X.J., Wang, S.T., 2018. ACS Appl. Mater. Interfaces 10, 42050–42057.
Xia, Y.K., Wang, L.L., Li, J., Chen, X.Q., Lan, J.M., Yan, A., Lei, Y., Yang, S., Yang, H.H., Chen, J.H., 2018. Anal. Chem. 90, 8969–8976.
Yang, H., Hui, A., Pampalakis, G., Soleymani, L., Liu, F.F., Sargent, E.H., Kelley, S.O., 2009. Angew. Chem. Int. Ed. 48, 8461–8464.
Yang, L., Wu, Q., Chen, Y.Q., Liu, X.Q., Wang, F.A., Zhou, X., 2019. ACS Sens. 4, 110–117.
Yi, J.T., Chen, T.T., Huo, J., Chu, X., 2017. Anal. Chem. 89, 12351–12359.
Yin, B.C., Liu, Y.Q., Ye, B.C., 2012. J. Am. Chem. Soc. 134, 5064–5067.